Oil production from waste polyethylene and polystyrene co-pyrolysis: Interactions of temperature and carrier gas flow rate

Ruming Pan, Yue Zan, Gerald Debenest

Oil production from waste polypropylene and polystyrene co-pyrolysis: Interactions of temperature and carrier gas flow rate

Ruming Pan[a,*], Yue Zan[b], Gérald Debenest[a]

[a]Institut de Mécanique des Fluides de Toulouse (IMFT) - Université de Toulouse, CNRS-INPT-UPS, Toulouse, 31400, France

[b]Laboratoire de Chimie de Coordination, CNRS UPR-8241 and Université de Toulouse, UPS, F-31077 Toulouse, France

Abstract: This study investigated the co-pyrolysis of waste polyethylene (WPE) and polystyrene (WPS) for oil production under different operating conditions (temperature and carrier gas flow rate). The ratio of the real-life WPE and WPS is different in different regions. Therefore, the interactions of operating conditions were investigated under different WPE/WPS mixture compositions. A hybrid model of artificial neural network-genetic algorithm (ANN-GA) was adopted to predict and optimize the co-pyrolysis oil yield due to the complex interactions of the WPE/WPS mixture composition and operating conditions. Consequently, the highest oil yield was 82.33wt% under 525℃, 10wt% PS, and a non-sweeping atmosphere (0mL/min). The results indicated that high temperature, low PS mass fraction, and low carrier gas flow rate led to a higher oil yield. The WPE/WPS co-pyrolysis oils were composed of alkanes, alkenes, and aromatics. Meanwhile, styrene accounted for the highest proportion of aromatics in oils. ANN-GA was also adopted to predict and optimize the

oil components and fractions. The results revealed that low temperature, high PS mass fraction, and low carrier gas flow rate were conducive to a light WPE/WPS co-pyrolysis oil production. The findings could guide the industrial process of waste plastic pyrolysis in different regions. Moreover, ANN-GA coupled with central-composite design can be used to regulate different target products under more complex conditions due to its good robustness.

Keywords: *Waste Plastic; Co-pyrolysis; Oil Production; Artificial neural network; Genetic algorithm.*

1. Introduction

The production of plastic has grown promptly from 1.5 million tons in 1950 to 368 million tons in 2019 [1]. The European plastic production was up to 57.9 million tons in 2019 [1], and almost half of the produced plastic became waste [2]. Moreover, nearly 25% of waste plastic winds up in landfills [3]. Consequently, waste plastic accumulates rapidly due to the low environmental degradability [4]. Plastic pollution destroys ecosystems [5] and causes harm to living creatures [6]. Pyrolysis is considered a promising alternative to landfill disposal of waste plastic, which can simultaneously produce liquid oil similar to commercial fuels (gasoline and diesel) [7-10]. Polyethylene (PE) and polystyrene (PS) are the first and third-most components in waste plastic due to their wide range of uses [11-12]. Therefore, many studies have investigated waste polyethylene (WPE) and polystyrene (WPS) pyrolysis for oil production. Park et al. [13] studied the pyrolysis of WPE at 653–736ºC and recovered

15–38wt% oil in a tandem two-stage reactor. Al-Salem et al. [7,14] conducted the low-density PE pyrolysis experiments at 500–800ºC. They found that the maximum wax yield was 64.5wt% at 500ºC [14], and the highest oil yield was 29wt% at 600ºC [7]. The WPS pyrolysis oil has been reported to have a higher yield than the WPE pyrolysis oil. Nisar et al. [15] recovered 44.9–86.1wt% oil from the pyrolysis of WPS at 340–420ºC. Quesada et al. [11] also obtained a high yield of 80wt% WPS thermal pyrolysis oil at 500ºC in a fixed bed reactor. It can be concluded that temperature is a critical parameter determining pyrolysis oil production.

WPE and WPS in waste plastic have different contents in different regions [3]. Therefore, the effect of WPE/WPS mixture composition on oil production has also been studied by researchers. Quesada et al. [11] investigated the WPE/WPS mixture (25wt% PS) co-pyrolysis at 500ºC and obtained ~70wt% of oil yield. Siddiqui and Redhwi [16] investigated the high-density-PE/PS (50–75wt% PS) co-pyrolysis at 440ºC in a batch reactor. It was found that as the PS mass fraction increased, the oil yield decreased from 72.8wt% (under 50wt% PS) to 25.6wt% (under 66.7wt% PS), while it increased to 56.1wt% when the PS mass fraction continuously increased to 75wt% PS. Williams and Williams [17] obtained 67.3wt% oil from PE/PS mixture (50wt% PS) co-pyrolysis at 700ºC. While the predicted oil yield, calculated by the PE and PS sole pyrolysis oil yields, was 81.7wt%. They concluded that an interaction between PE and PS led to a lower-than-expected oil yield. Klaimy et al. found that the co-pyrolysis of plastic mixtures promoted the production of lightweight components (C6 and C7) in the oil [18]. Saad et al. [19] suggested that PE and PS could be fully decomposed before

500ºC with a heating rate of 10ºC/min. However, the plastic compositions affected the activation energies of mixed plastics. Moreover, co-pyrolysis of other types of plastics [20] and co-pyrolysis of plastics with biomass [21] also found the complex interactive effects of the mixture compositions.

On the other hand, the carrier gas flow rate is a significant parameter during the pyrolysis of plastic [22-23]. Muhammad et al. [23] investigated the effect of carrier gas flow rate on the pyrolysis of linear low-density PE. They found that increasing the flow rate from 0mL/min to 1mL/min could dramatically enhance the oil yield from 54.0wt% to 61.5wt%. In contrast, the oil yield decreased to 45.0wt% under the flow rate of 60mL/min. Pan et al. [22] concluded that the WPE pyrolysis oil yield would decrease from 82.43wt% to 65.32wt% when the flow rate increased from 20mL/min to 100mL/min.

It can be concluded that the temperature and the carrier gas flow rate are two vital parameters during plastic pyrolysis. The WPE/WPS mixture composition also has a non-linear effect on the co-pyrolysis oil yield. The artificial neural network (ANN) is a promising method to formulate the dependent variable in terms of independent variables with complex interactions [24]. Neshat et al. [25-26] adopted ANN to predict wind speed and wind turbine power output. The findings revealed that ANN could accurately establish the expressions of the dependent variables. ANN can also be competent for detection works, e.g., plate's structural damage [27] and COVID-19 [28]. An optimization algorithm is required to determine the extrema of complex mathematical expressions established by the ANN. Genetic algorithm (GA), inspired by the evolution theory, is a widely used optimization algorithm [29].

Furthermore, GA has been proven to be qualified to determine the extrema of ANN-established expression [30].

The primary aim of this study is to investigate the interactions of operating conditions (temperature and flow rate of carrier gas) on the WPE/WPS (with different mixture compositions) co-pyrolysis oil yield. A hybrid model of the artificial neural network coupled with a genetic algorithm (ANN-GA) is adopted to quantitatively describe the complex interactions of operating conditions and WPE/WPS mixture composition on the product yields based on the experimental results. The oil samples are analyzed by gas chromatography/mass spectrometry (GC/MS) to determine the specific components. The ANN-GA is also adopted to predict and optimize the oil components and fractions under different operating conditions and WPE/WPS mixture compositions. The findings can guide the regional industrialization of waste plastic pyrolysis.

2. Experiments and method

2.1. Pyrolysis experiments

WPE and WPS were recycled from municipal solid waste (MSW) and provided by Zhoushan Jinke Renewable Resources Co., China. The waste plastics were first collected and sorted, then washed and dried, and finally made into pellets of about 3mm. The total mass of the WPE/WPS mixture used in each pyrolysis experiment was ~5g. As shown in Fig. 1, the WPE/WPS co-pyrolysis experiments were carried out in a 200mL semi-batch reactor. The WPE/WPS samples were mixed well and placed in the Al_2O_3 crucible. The reactor was

purged with nitrogen (under 100mL/min) for 30min to ensure an inert atmosphere. The reactor was heated to the target temperature at 6℃/min and stayed at the target temperature for 20min. Two in-tandem glass bottles collected the WPE/WPS pyrolysis oil in a mixture of ice and water. A gas bag collected the pyrolysis gas. The char remained in the Al_2O_3 crucible and was collected after cooling the reactor to 20℃.

The temperature, PS mass fraction, and flow rate of carrier gas were studied in the ranges of 425–525℃ [19,22,31], 10–30wt% PS [3], and 0–60mL/min [23] based on the plastic pyrolysis characteristics, regional WPE/WPS composition, and reactor size. The WPE/WPS co-pyrolysis experiments were designed according to the central-composite design [32] and tabulated in Table A.1. 17 sets of experiments (R1–R17) were conducted to obtain the training set data of ANN-GA. 5 sets of experiments (R18–R22) were carried out to get the testing set data of ANN-GA. Moreover, the WPE/WPS co-pyrolysis oil samples were characterized by GC/MS to determine the specific composition of the oil.

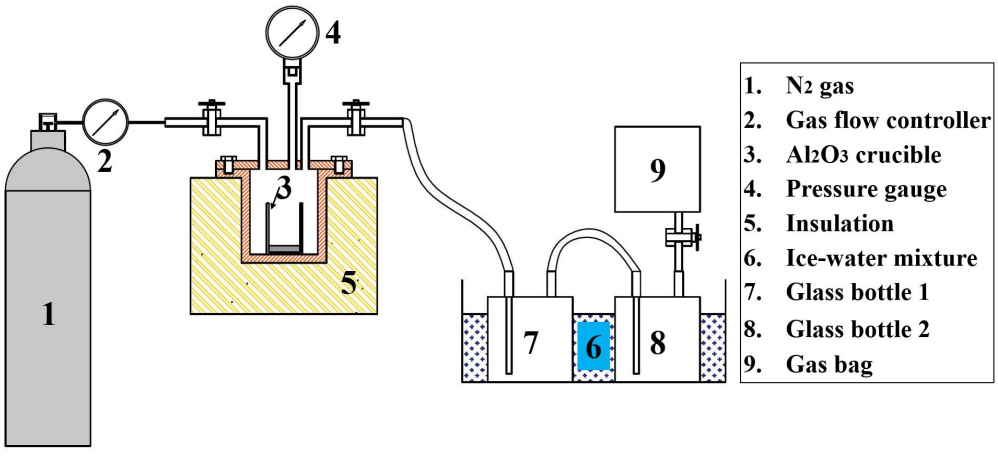

Fig. 1. The WPE/WPS co-pyrolysis experimental setup.

2.2. Method

A hybrid artificial neural network model coupled with a genetic algorithm (ANN-GA) was adopted to predict and optimize the WPE/WPS co-pyrolysis product yields, oil components, and fractions. The simulation platform of the ANN-GA is Matlab R2016a. Fig. 2 demonstrates the flow chart of ANN-GA. The mathematical expressions of ANN-GA have been detailed described in the previous study [30]. The arithmetic expressions between the independent (temperature, PS mass fraction, and flow rate of carrier gas) and dependent variables (co-pyrolysis product yields, oil components, and fractions) were established by ANN based on the experimental results [33]. Subsequently, GA was used to optimize the objective functions built by ANN. Consequently, the conditions (temperature, PS mass fraction, and carrier gas flow rate) for the highest oil yield and the lightest oil production could be determined by ANN-GA.

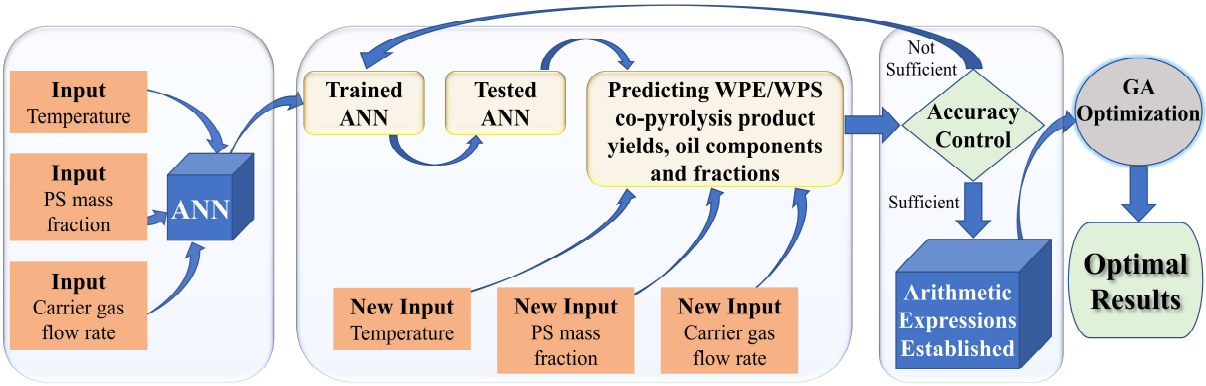

Fig. 2. The flow chart of ANN-GA.

3. Results and discussion

3.1. Accuracy of ANN predicted co-pyrolysis product yields

Fig. 3 shows the experimental and ANN predicted WPE/WPS co-pyrolysis oil, gas, and char yields. It can be seen that the experimental oil yield varied from 61.51wt% (Sample R4)

to 82.28wt% (Sample R13), the experimental gas yield fluctuated from 10.01wt% (Sample R1) to 18.65wt% (Sample R17), and the experimental char yield oscillated from 3.93wt% (Sample R21) to 8.92wt% (Sample R5). It was reported that the WPE thermal pyrolysis oil and gas yields were 65.32–83.50wt% and 11.50–18.75wt% in the temperature range of 425–525ºC [22]. The PS thermal pyrolysis oil yields were 80wt% under 450ºC [34] and 71wt% under 500ºC [35]. Moreover, the WPS pyrolysis gas and char yields were ~16wt% and ~4wt% under 500ºC, respectively [11]. The WPE/WPS co-pyrolysis product yields obtained in the present work were within the ranges of individual WPE and WPS pyrolysis ones. Quesada et al. [11] studied the WPE/WPS co-pyrolysis under 500ºC and 25wt% PS, obtaining ~70wt% of oil yield, ~22wt% of gas yield, and ~8wt% of char yield, values highly close to that obtained in the present work. Williams and Williams [17] obtained 64.0–67.3wt% oil yield and 1.2–2.2wt% char yield from PE/PS co-pyrolysis, which were also very close to the results in the present work.

On the other hand, Table 1 lists the root mean square error (RMSE), mean relative error (MRE), mean absolute error (MAE), standard deviation (SD), and coefficient of determination (R2) values between the experimental and ANN predicted co-pyrolysis product yields in the training and testing sets. The high R2 values and low RMSE, MRE, MAE, and SD values [36] exhibited the high accuracy of the ANN predicted WPE/WPS co-pyrolysis product yields.

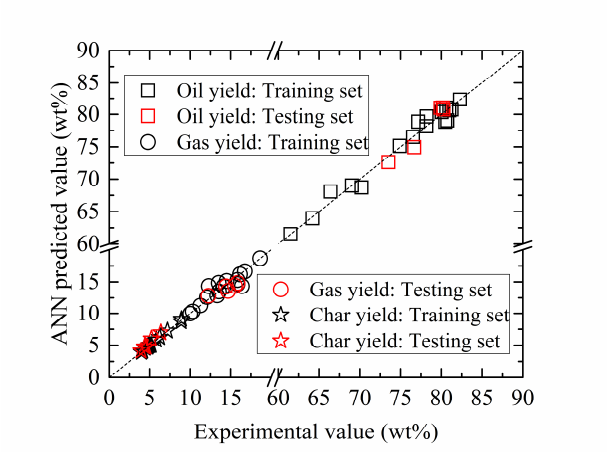

Fig. 3. Experimental and ANN predicted co-pyrolysis product yields.

Table 1. Errors in the ANN predicted co-pyrolysis product yields.

	RMSE`	MRE	MAE	SD	R2
Training set	0.76%	-0.14%	2.06%	3.23%	0.9994
Testing set	0.87%	-1.60%	5.07%	4.03%	0.9993

3.2. Interactions of temperature, PS mass fraction, and carrier gas flow rate on product yields

Fig. 4 demonstrates the interactions of temperature, PS mass fraction, and carrier gas flow rate on the distributions of oil, gas, and char productions under 0mL/min, 10wt% PS, and 425℃. It is worth noting that due to the pressure difference generated during the pyrolysis of plastics, oil and gas can flow out of the reactor spontaneously under 0mL/min. Moreover, Figs. A.1–3 illustrate the ANN predicted oil, gas, and char yields under 30mL/min and 60mL/min, 20wt% PS and 30wt% PS, and 475℃ and 525℃, respectively. It could be seen that the temperature had a more significant impact on the oil yield than the PS mass fraction under all flow rates of carrier gas (Fig. 4a, Fig. A.1a, and Fig. A.1d). Quesada et al. [11] also reported

that the WPE/WPS co-pyrolysis oil yield only hovered in a narrow range of ~70–73wt% within the range of 25–75wt% PS. As the temperature increased, the oil yields were significantly enhanced by 18.35wt% (under 10wt% PS) and 16.65wt% (under 30wt% PS) under the non-sweeping atmosphere (0mL/min, Fig. 4a). Higher temperatures could deepen the random scissions of WPE/WPS long chains [37] and the secondary cracking of char [38-39], thereby enhancing oil and gas yields and reducing char yield. Increasing the temperature further would cause the secondary reactions of oil cracking [15,40], and gas recondensation and repolymerization [17]. Therefore, when the temperature exceeded 480℃ and continued to rise, the decrease in gas yield under 0mL/min (Fig. 4b) could be ascribed to the gas recondensation and repolymerization (gas consumption) were more intense than the oil cracking (gas generation). However, as the temperature increased from 488℃, the decrease in oil yield under 30mL/min (Fig. A.1a) and 60mL/min (Fig. A.1d) might be attributed to the oil cracking (oil consumption) was more violent than the gas recondensation and repolymerization (oil formation) [14].

Improving the flow rate of carrier gas under low temperatures would enhance the oil and gas yields, regardless of the variation of PS mass fraction. For instance, the oil and gas yields were enhanced by 4.76wt% and 2.90wt% under 425℃ and 10wt% PS (Fig. 4d). However, increasing the carrier gas flow rate decreased the oil yield by ~2wt% under the highest temperature (525℃). The reduction of the oil yield might be ascribed to the shorter residence time of volatile products in the reaction zone under higher flow rates of carrier gas, thereby inhibiting the Diels-Alder reactions of gaseous olefin for oil formation [41]. Simultaneously,

196 the gas yield was enhanced by 1.80wt% (13.50wt%–15.30wt%) as the flow rate of carrier gas
197 increased under 525ºC (Fig. 4e). On the other hand, the carrier gas flow rate's increase led to a
198 decrease in char yield under high temperatures. As the flow rate of carrier gas increased, the
199 char yields reduced by 0.09wt%, 0.15wt%, and 0.17wt% under 10wt% PS (Fig. 4f), 20wt%
200 PS (Fig. A.2c), and 30wt% PS (Fig. A.2f), respectively. The decrease in char yield could be
201 ascribed to the inhabitation of secondary reactions of the co-pyrolysis volatiles for char
202 generation [42]. However, enhancing the carrier gas flow rate increased the char yield under
203 lower temperatures. The flow rate change would affect the heat transfer efficiency in the
204 reaction zone [43], which might enhance the char yield.

205 Enhancing the PS mass fraction in WPE/WPS led to a decrease in oil yield and an
206 increase in gas and char yields under the non-sweeping atmosphere (0mL/min). For instance,
207 the enhancement of PS mass fraction led to a reduction of 2.46wt% in oil yield (Fig. 4g), an
208 enhancement of 0.35wt% in gas yield (Fig. 4h), and an enhancement of 0.40wt% in char yield
209 (Fig. 4i) under 425ºC and 0mL/min. Similar trends were reported by Quesada et al. [11]: a
210 decrease of ~3.5wt% in oil yield, an increase of ~1.5wt% in gas yield, and an increase of
211 ~2wt% in char yield were observed when the PS mass fraction increased from 50wt% to
212 75wt% in WPE/WPS. The increase in char yield might be ascribed to the abundant aromatics
213 presented in the PS pyrolysis oil, which could further generate char [15].

214

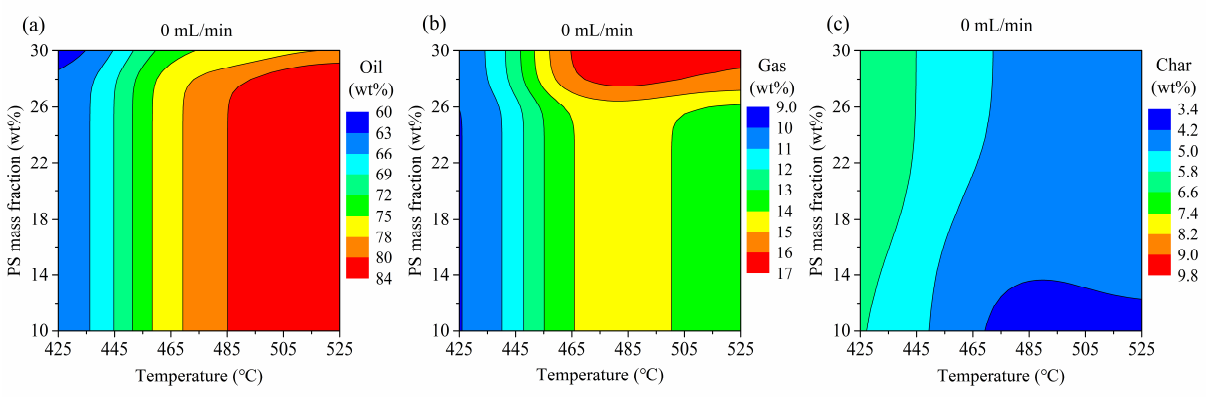

215

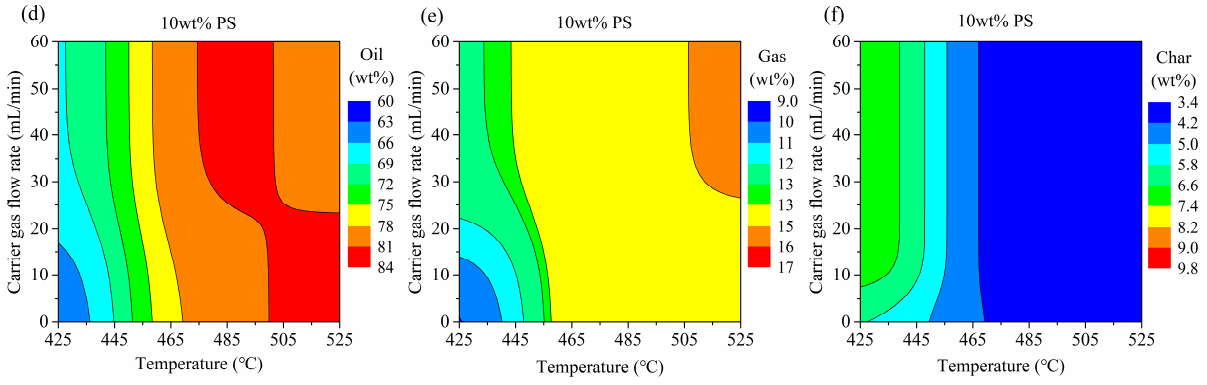

216

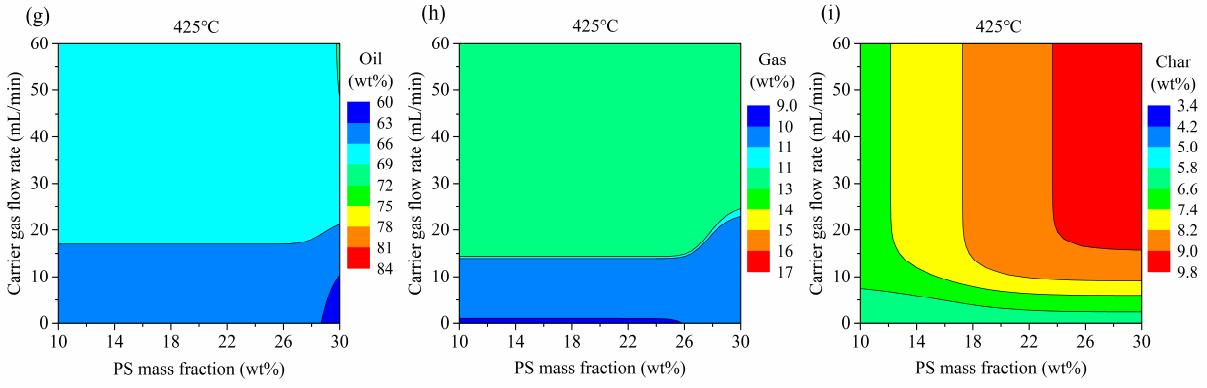

217 **Fig. 4.** Interactive effects of temperature, PS mass fraction, and carrier gas flow rate on the distributions of

218 WPE/WPS co-pyrolysis products: (a) Oil yield under 0mL/min; (b) Gas yield under 0mL/min; (c) Char

219 yield under 0mL/min; (d) Oil yield under 10wt% PS; (e) Gas yield under 10wt% PS; (f) Char yield under

220 10wt% PS; (g) Oil yield under 425℃; (h) Gas yield under 425℃; (i) Char yield under 425℃.

221

222 *3.3. Optimization of oil yield by ANN-GA*

Fig. 5a shows the optimal and average values of the ANN-GA objective function (oil yield). The ANN-GA predicted the highest oil yield was 82.33wt% under 525ºC, 10wt% PS, and 0mL/min (Fig. 5b). Meanwhile, the experimental oil yield under the ANN-GA optimized conditions was 82.28wt%. The relative error between the experimental and ANN-GA predicted oil yields was merely 0.06%, revealing the ANN-GA optimized value's high accuracy.

It is also noteworthy that the highest oil yield under 60mL/min was obtained at 485ºC. The optimal temperature of 485ºC was close to the optimal WPE pyrolysis temperatures reported by Quesada et al. [31] (500ºC) and Pan et al. [22] (488ºC). Carrier gas could accelerate the purging of the pyrolysis volatiles and carry heavier volatile molecules out of the reactor. The heavy pyrolysis oil components remained in the reactor under the non-sweeping atmosphere (0mL/min). Higher temperatures were required for the thermal cracking of oil's heavy components into shorter-chain hydrocarbons, which then could volatilize and spontaneously leave the reactor [44]. Therefore, WPE/WPS co-pyrolysis oil yield optimized temperature exceeded 500ºC, generally considered the optimal temperature for the pyrolysis of waste plastics with carrier gas [45].

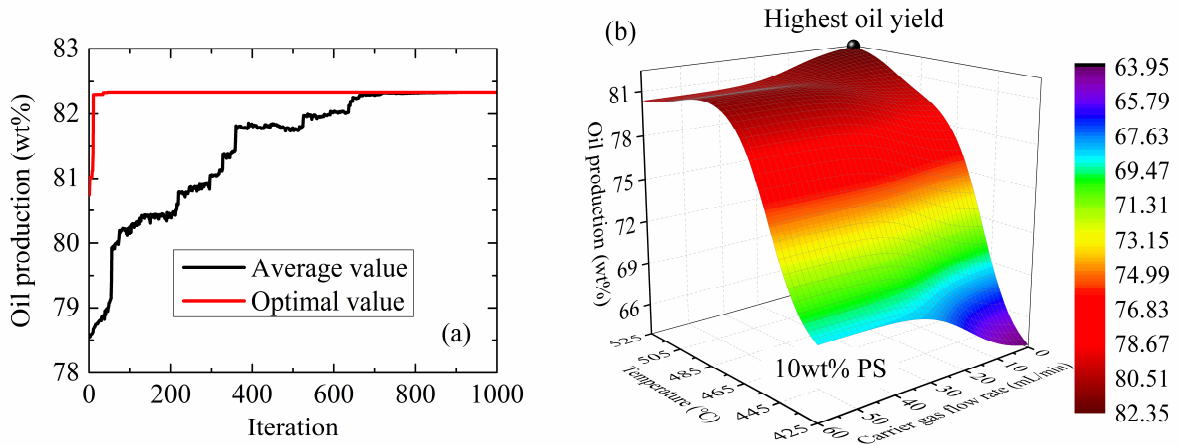

Fig. 5. Optimization of oil yield by ANN-GA: (a) Representation of optimization process; (b) Highest oil yield.

3.4. GC/MS analysis

The components of WPE/WPS co-pyrolysis oil samples (R1–R22) were analyzed by GC/MS. Moreover, the WPE/WPS co-pyrolysis oils were divided into light (C7–C11), middle (C12–C20), and heavy fractions (>C20) based on the carbon numbers [22]. Fig. 6a indicates that the oils were composed of alkanes (24.55–48.25%), alkenes (29.38–52.57%), and aromatics (9.68–42.89%) [11]. Meanwhile, styrene accounted for the highest proportion of aromatics in oils, which varied from 26.73% to 54.87%. High styrene proportion might be ascribed to aromatic hydrocarbons that take up the main component of WPS thermal pyrolysis oil, of which styrene occupies 33–40% [46].

Fig. 6b shows that the light, middle, and heavy oil fractions fluctuated from 18.49–48.49%, 35.32–56.78%, and 13.64–37.05%, respectively. The WPE/WPS co-pyrolysis oils had more light and middle fractions than WPE pyrolysis oils [22]. Moreover, the mean molecular weight of the WPE/WPS co-pyrolysis oil oscillated from 187.73g/mol to 251.01g/mol, which was between the mean molecular weights of individual PS (176g/mol) and PE (306g/mol) thermal pyrolysis oils [17].

The operating conditions of temperature and carrier gas flow rate had complex interactions on the WPE/WPS co-pyrolysis oil components and fractions [47]. Moreover, the styrene/aromatics ratio and the mean molecular weight of WPE/WPS co-pyrolysis oil did not

linearly change as the PS mass fraction increased [16]. The non-linear relationship indicated that the reaction species of WPE and WPS had undetermined interactions on the distributions of co-pyrolysis oil components and fractions [17]. Therefore, ANN-GA was adopted to investigate the interactions of temperature, PS mass fraction, and carrier gas flow rate on the oil components and fractions; and determine the optimal conditions for each component and fraction.

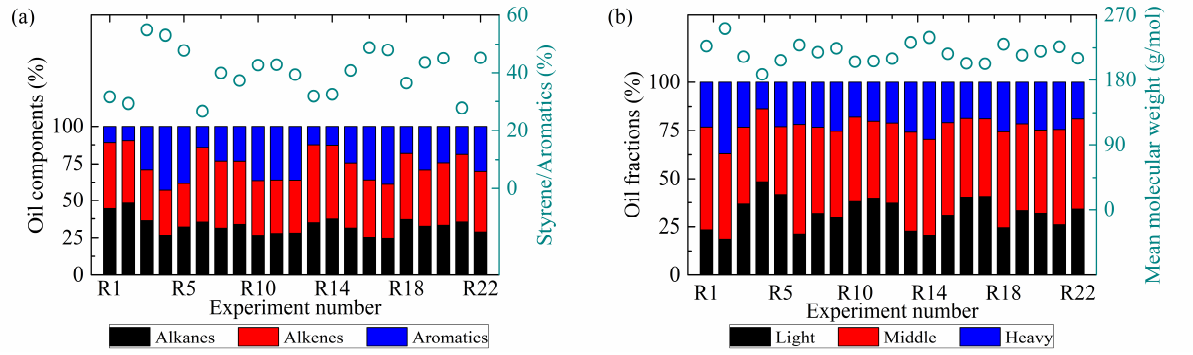

Fig. 6. WPE/WPS co-pyrolysis oil components and fractions: (a) Distributions of alkanes, alkenes, and aromatics in oils, and the styrene/aromatics ratio variations; (b) Distributions of light, middle, and heavy fractions in oils, and the mean molecular weight variations.

3.5. WPE/WPS co-pyrolysis oil components

3.5.1. Interactions of temperature, PS mass fraction, and carrier gas flow rate

Fig. 7 demonstrates the experimental and ANN predicted oil components in the training and testing sets. Besides, Table 2 tabulates the RMSE, MRE, MAE, SD, and R2 values between the experimental and ANN predicted oil components. The high R2 values and low RMSE, MRE, MAE, and SD values verified the accuracy of predicted results.

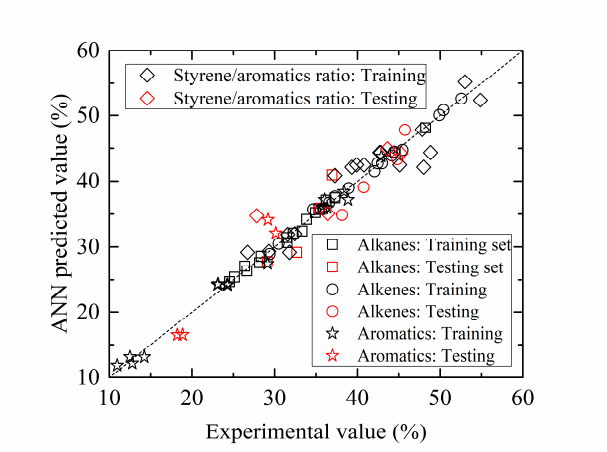

278

279 **Fig. 7.** Experimental and ANN predicted oil components.

280

281 **Table 2.** Errors in the ANN predicted oil components.

	RMSE`	MRE	MAE	SD	R2
Training set	1.44%	-0.16%	2.60%	3.38%	0.9798
Testing set	2.96%	-0.53%	7.97%	3.39%	0.8762

282

283 Fig. 8 shows the interactions of temperature, PS mass fraction, and carrier gas flow rate
284 on the distributions of oil components under 0mL/min, 10wt% PS, and 425℃. The
285 interactions of triple conditions under 30mL/min, 20wt% PS, and 475℃ (Fig. A.5); and
286 60mL/min, 30wt% PS, and 525℃ (Fig. A.7) are similar to the conditions under 0mL/min,
287 10wt% PS, and 425℃. It could be observed that the temperature had a more significant
288 influence on the alkanes proportion under lower PS mass fractions (Fig. 8a). As the
289 temperature increased under 10wt% PS, the alkanes proportion reduced by 9.10% (44.31%–
290 35.21%, Fig. 8a), while the alkanes proportion enhanced by 8.12% (44.45%–52.57%, Fig. 8b).
291 Increasing temperature contributed to a decrease of 7.87% (43.73%–35.86%) in aromatics
292 proportion under 30wt% PS (Fig. 8c). Aromatics were mainly generated from the thermal

293 decomposition of PS in WPE/WPS. The polycyclic PS could be decomposed under a lower
294 temperature than PE [48], thereby a high aromatics proportion of 43.73% was obtained under
295 425ºC, 30wt% PS, and 0mL/min (Fig. 8c). Enhancing the temperature aggravates the
296 secondary cracking reactions of alkanes and aromatics for the generation of alkenes, leading
297 to a decrease in alkanes and aromatics proportions and an increase in alkenes proportion [49].
298 Figs. 8d–f demonstrate the interactions of carrier gas flow rate and temperature on the
299 proportions of alkanes, alkenes, and aromatics under 10wt% PS, respectively. It could be seen
300 that improving the flow rate of carrier gas would enhance the alkanes proportion and reduce
301 the alkenes and aromatics proportions under all temperatures. For instance, as the flow rate of
302 carrier gas increased under 525ºC and 10wt% PS, the alkanes proportion increased by 2.25%
303 (35.21%–37.46%), while the alkenes and aromatics proportions decreased by 2.51%
304 (52.57%–50.06%) and 0.94% (13.11%–12.17%), respectively. Higher carrier gas flow rates
305 could purge the co-pyrolysis volatiles out of the reaction zone faster [50], thereby suppressing
306 the secondary cracking of alkanes for alkenes formation and the Diels-Alder reactions of
307 alkenes for aromatics formation [41].
308 On the other hand, as the PS mass fraction increased, the alkanes and alkenes proportions
309 reduced by ~16–18% (Fig. 8g) and ~12.6–14% (Fig. 8h), while the aromatics proportion
310 significantly enhanced by ~29–32% (Fig. 8i) under 425ºC. The principal components of PS
311 pyrolysis oil were aromatics [51], thereby enhancing the PS mass fraction led to an increase in
312 aromatics proportion and a decrease in alkanes and alkenes proportions.

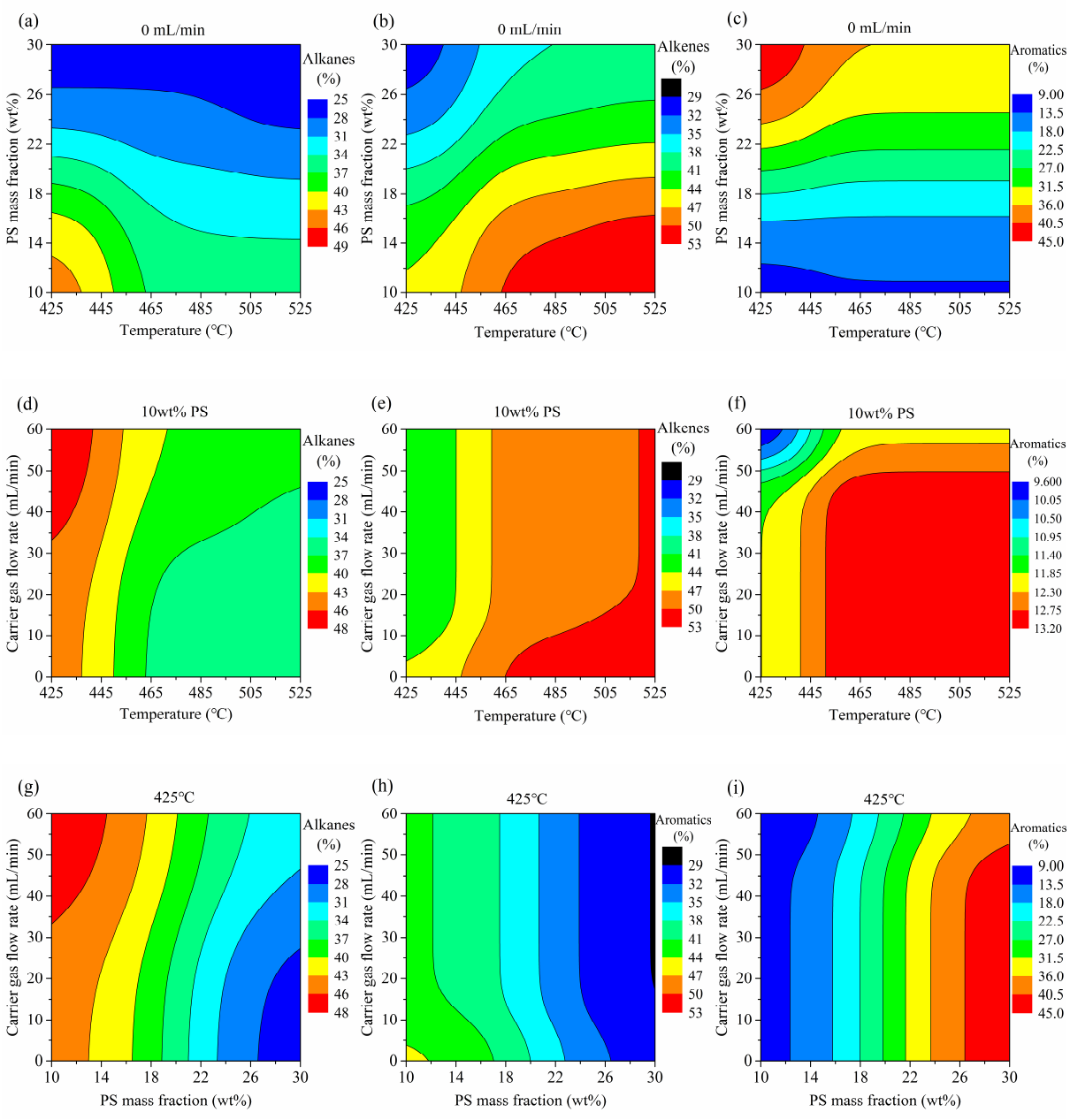

Fig. 8. Interactive effects of temperature, PS mass fraction, and carrier gas flow rate on the distributions of WPE/WPS co-pyrolysis oil components: (a) Alkanes proportion under 0mL/min; (b) Alkenes proportion under 0mL/min; (c) Aromatics proportion under 0mL/min; (d) Alkanes proportion under 10wt% PS; (e) Alkenes proportion under 10wt% PS; (f) Aromatics proportion under 10wt% PS; (g) Alkanes proportion under 425℃; (h) Alkenes proportion under 425℃; (i) Aromatics proportion under 425℃.

Styrene was the dominant component in the WPE/WPS co-pyrolysis oil's aromatics proportion, which could be ascribed to the primary product of styrene in the PS pyrolysis oil [16,46]. Fig. 9 depicts the interactions of temperature, PS mass fraction, and carrier gas flow rate on the styrene/aromatics ratio under 0mL/min, 30wt% PS, and 425ºC. Moreover, Fig. A.6 and Fig. A.8 demonstrate the interactions of triple conditions under 30mL/min, 20wt% PS, and 475ºC; and 60mL/min, 10wt% PS, and 525ºC, respectively. The enhancement of PS mass fraction contributed to the increases of ~26%, ~26%, and ~19% in styrene/aromatics ratio under 0mL/min (Fig. 9a), 30mL/min (Fig. A.6a), and 60mL/min (Fig. A.8a), respectively. The temperature had a more significant impact on the styrene/aromatics ratio under 20wt% (Fig. A.6b) and 30wt% (Fig. 9b) PS mass fractions compared to the one under 10wt% PS mass fraction (Fig. A.8b). Besides, the increase in temperature under 20wt% and 30wt% PS mass fractions resulted in a reduction of styrene/aromatics ratio, which might be ascribed to the secondary cracking of styrene under higher temperatures [52]. On the other hand, improving the flow rate of carrier gas led to a decrease in styrene/aromatics ratio under 425ºC (Fig. 9c), regardless of the variation of PS mass fraction. Higher carrier gas flow rates would shorten the volatiles residence time in the reaction zone, thereby resulting in the incomplete pyrolysis of PS for styrene formation.

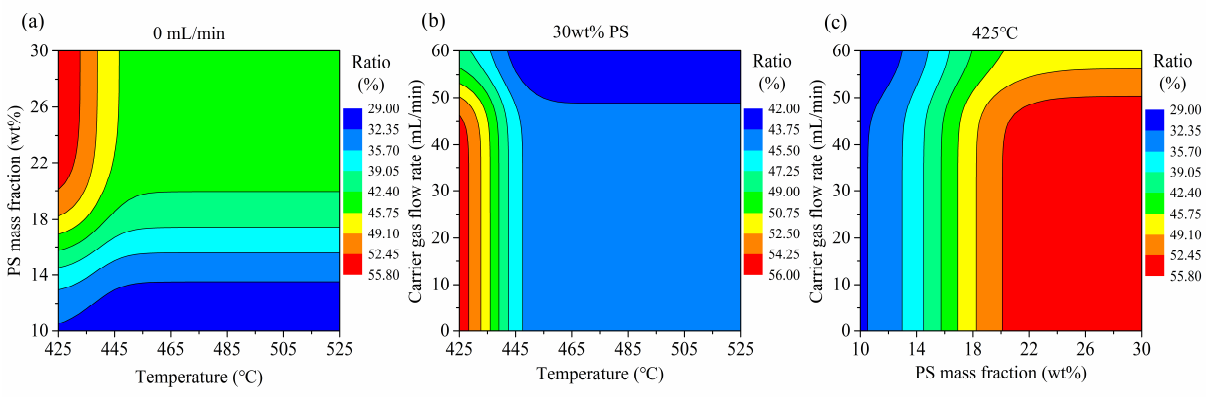

Fig. 9. Interactive effects of temperature, PS mass fraction, and carrier gas flow rate on the styrene/aromatics ratio: (a) Under 0mL/min; (b) Under 30wt% PS; (c) Under 425℃.

3.5.2. ANN-GA optimization

Fig. 10a shows that the highest alkanes proportion was 48.09% under 425℃, 10wt% PS, and 60mL/min, which indicated that low temperature and high carrier gas flow rate could suppress the secondary cracking of alkanes in oil [53-56]. On the other hand, the highest alkenes proportion was 52.57% under 525℃, 10wt% PS, and the non-sweeping atmosphere (0mL/min). High temperature and low carrier gas flow rate resulted in the over-cracking of the oil, which might be conducive to the formation of alkene.

The highest aromatics proportion of 43.73% was obtained under 425℃, 30wt% PS, and 0mL/min. Increasing temperature can affect the aromatics proportion in three aspects: i) promoting the alkanes' dehydro-aromatization [57] for aromatics formation, ii) facilitating the alkenes' Diels-Alder reactions [41] for aromatics formation, and iii) exacerbating the over-cracking for aromatics consumption [49]. The highest aromatics proportion achieved under low temperature indicated that the inhibition of aromatics over-cracking dominated the

aromatics formation. High PS mass fraction in the WPE/WPS mixture could enhance the proportion of the aromatics; thereby, the highest aromatics proportion was gained under 30wt% PS. Meanwhile, the highest styrene/aromatics ratio was 55.22% under the same conditions (425℃, 30wt% PS, and 0mL/min). This was because styrene was the dominant component in the PS pyrolysis oil.

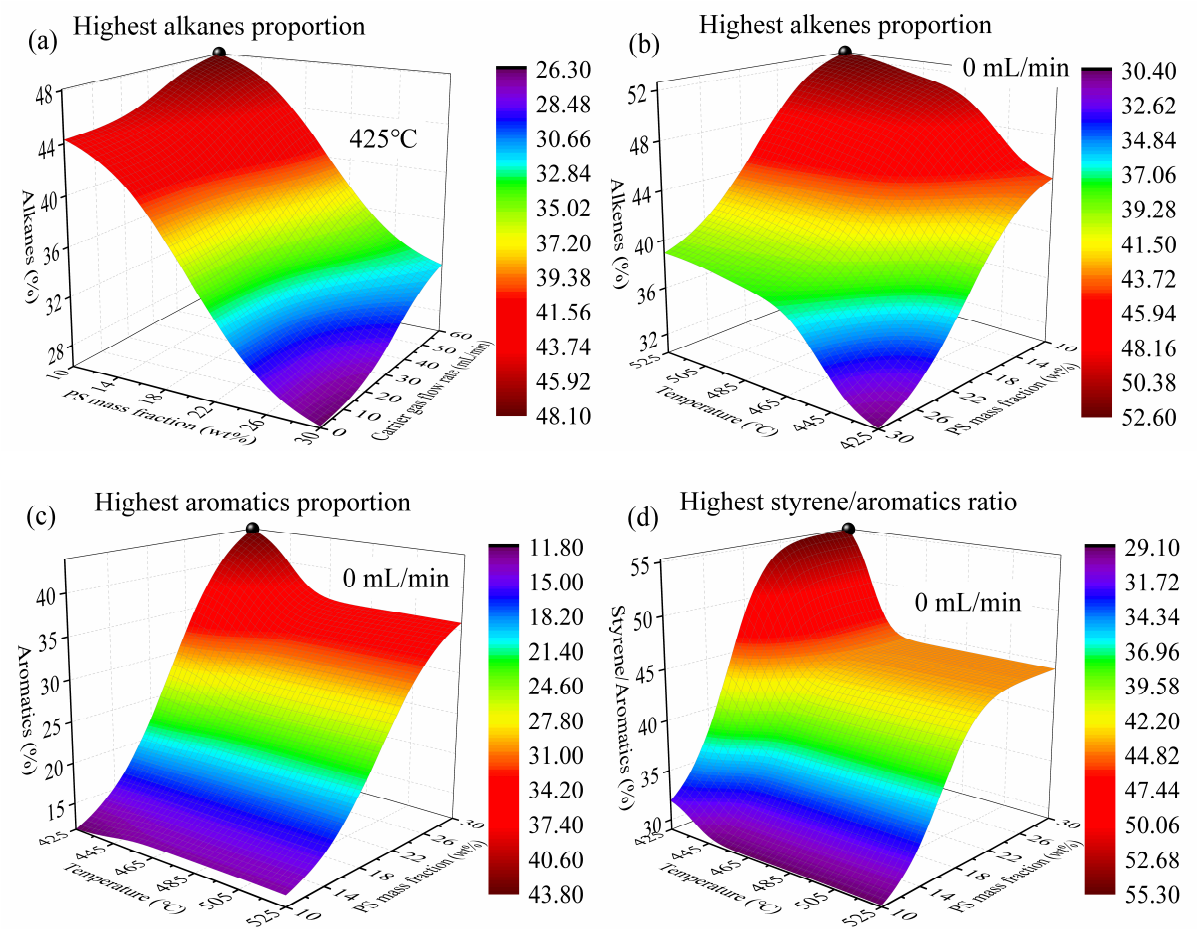

Fig. 10. ANN-GA optimized proportions of the oil components and styrene/aromatics ratio: (a) Highest alkanes proportion; (b) Highest alkenes proportion; (c) Highest aromatics proportion; (d) Highest styrene/aromatics ratio.

3.6. WPE/WPS co-pyrolysis oil fractions

3.6.1. Interactions of temperature, PS mass fraction, and carrier gas flow rate

Fig. 11 shows the experimental and ANN predicted oil fractions in the training and testing sets. Moreover, Table 3 lists the RMSE, MRE, MAE, SD, and R2 values between the experimental and ANN predicted oil fractions. The high R2 values and low RMSE, MRE, MAE, and SD values exhibited high accuracy of the predicted results.

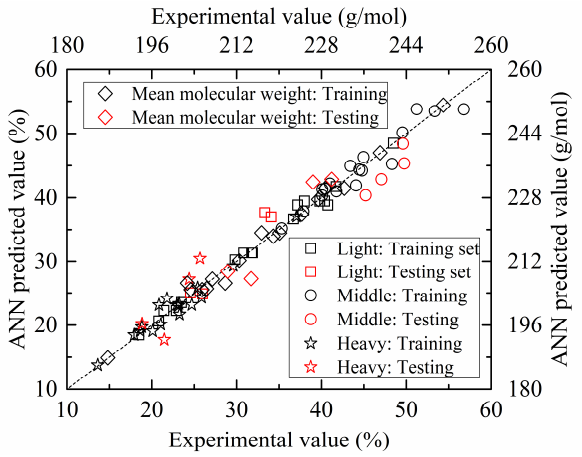

Fig. 11. Experimental and ANN predicted oil fractions.

Table 3. Errors in the ANN predicted oil fractions.

	RMSE`	MRE	MAE	SD	R2
Training set	1.38%	-0.09%	2.00%	2.91%	0.9995
Testing set	3.38%	-1.77%	6.88%	3.22%	0.9970

Fig. 12 depicts the interactions of temperature, PS mass fraction, and carrier gas flow rate on the distributions of oil fractions under 0mL/min, 10wt% PS, and 425℃. The interactions of triple conditions under 30mL/min, 20wt% PS, and 475℃ (Fig. A.11); and 60mL/min, 30wt% PS, and 525℃ (Fig. A.13) are similar to the conditions under 0mL/min, 10wt% PS, and 425℃. Figs. 12a–c demonstrate that the temperature significantly impacted the oil fractions under

383 higher PS mass fractions. As the temperature increased under 10wt% PS, the light fraction
384 decreased by 1.24%, and the middle and heavy fractions increased by 0.31% and 1.30%,
385 respectively. However, the light fraction significantly reduced by 9.03%, and the middle and
386 heavy fractions enhanced by 4.32% and 5.35% when the temperature increased under 30wt%
387 PS. Higher temperatures could aggravate the secondary cracking of light fraction in oil,
388 thereby reducing the light fraction and enhancing the middle and heavy fractions [58].

389 It is noteworthy that the light and middle fractions would decrease, and the heavy fraction
390 would increase as the flow rate of carrier gas increased, regardless of the variations of
391 temperature and PS mass fraction (Figs. 12d–f). For instance, the carrier gas flow rate's
392 increase reduced the light (by 5.02%) and middle (by 9.10%) fractions, and enhanced the
393 heavy fraction (by 14.05%) under 425℃ and 10wt% PS, respectively. It might be ascribed to
394 the suppression of gas recondensation and repolymerization for generating the light and
395 middle fractions in oil under higher carrier gas flow rates.

396 On the other hand, enhancing the PS mass fraction could considerably increase the light
397 fraction and decrease the middle and heavy fractions in oil. For example, as the PS mass
398 fraction enhanced under 425℃ and non-sweeping atmosphere (0mL/min), the light fraction
399 increased by 24.99% (23.51%–48.50%), whereas the middle and heavy fractions decreased by
400 15.62% (53.48%–37.86%) and 9.23% (22.99%–13.76%), respectively. It might be ascribed to
401 the high proportion of styrene in the PS pyrolysis oil [11], which belonged to the light fraction.
402 Consequently, a higher PS mass fraction could contribute to an increase in the light fraction.

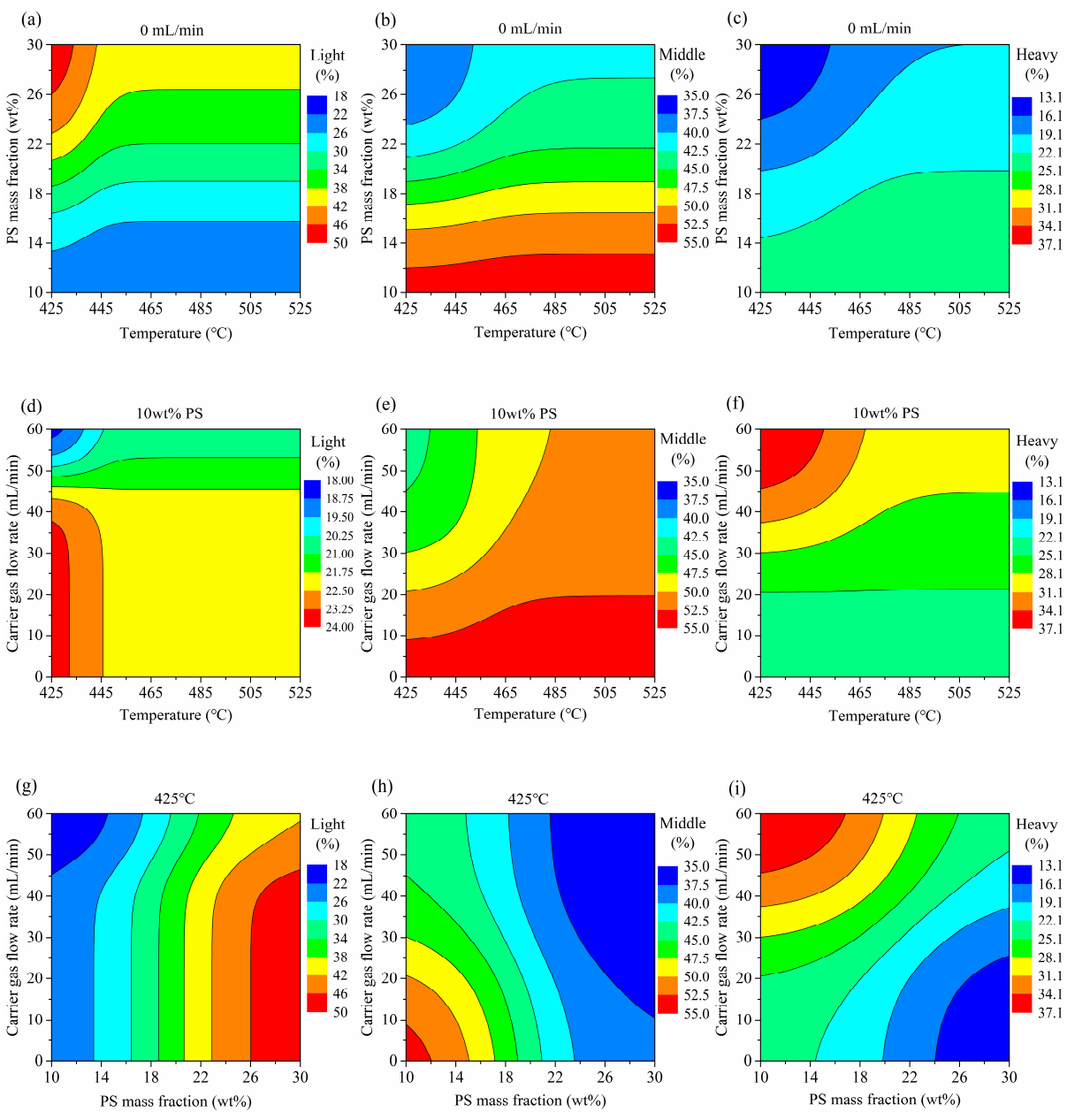

Fig. 12. Interactive effects of temperature, PS mass fraction, and carrier gas flow rate on the distributions of oil fractions: (a) Light fraction under 0mL/min; (b) Middle fraction under 0mL/min; (c) Heavy fraction under 0mL/min; (d) Light fraction under 10wt% PS; (e) Middle fraction under 10wt% PS; (f) Heavy fraction under 10wt% PS; (g) Light fraction under 425℃; (h) Middle fraction under 425℃; (i) Heavy fraction under 425℃.

Fig. 13 depicts the interactions of temperature, PS mass fraction, and carrier gas flow rate on the oil's mean molecular weight under 0mL/min, 10wt% PS, and 425ºC. Moreover, Fig. A.12 and Fig. A.14 demonstrate the interactions of triple conditions under 30mL/min, 20wt% PS, and 475ºC; and 60mL/min, 30wt% PS, and 525ºC, respectively. Fig. 13a shows that the oil's mean molecular weight increased with the increasing temperature under all PS mass fractions. Moreover, the temperature significantly impacted the oil's mean molecular weight under higher PS mass fractions. For instance, as the temperature increased under 0mL/min, the oil's mean molecular weight was enhanced by 2.77g/mol and 16.98g/mol under 10wt% PS and 30wt% PS, respectively. The enhancement might be due to the more intense over-cracking reaction of the oil's light fraction [59], producing a heavier oil with a higher mean molecular weight. A higher carrier gas flow rate increased the oil's mean molecular weight under all temperatures (Fig. 13b). The increase was because the light and middle fractions decreased, whereas the heavy fraction increased with the increasing flow rate of carrier gas (Figs. 12d–f). Besides, the increase in PS mass fraction contributed to a significant decrease of ~40g/mol in the oil's mean molecular weight under 425ºC (Fig. 13c).

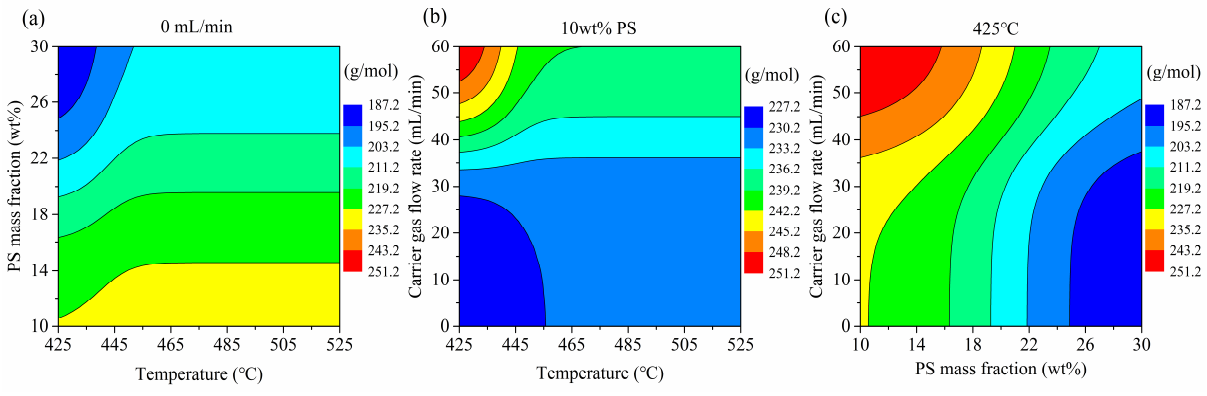

Fig. 13. Interactive effects of temperature, PS mass fraction, and carrier gas flow rate on the oil's mean

molecular weight: (a) Under 0mL/min; (b) Under 10wt% PS; (c) Under 425ºC.

3.6.2. ANN-GA optimization

As discussed in Section 3.6.1, the temperature, PS mass fraction, and carrier gas flow rate had complex interactions on the distributions of WPE/WPS co-pyrolysis oil fractions and the oil's mean molecular weight. Therefore, the ANN-GA was adopted to determine the highest oil fractions and the lightest co-pyrolysis oil with the lowest mean molecular weight.

Fig. 14a shows that the highest light fraction was 48.50% under 425ºC, 30wt% PS, and 0mL/min. Low temperature and non-sweeping atmosphere could suppress the secondary cracking of light fraction and promote gas recondensation for light fraction formation. The highest middle fraction of 53.79% was obtained under 525ºC, 10wt% PS, and 0mL/min (Fig. 14b). Higher temperatures might be conducive to the secondary cracking of heavy fraction for middle fraction generation. On the other hand, the highest heavy fraction was 37.04% under 425ºC, 10wt% PS, and 60mL/min (Fig. 14c).

The lightest WPE/WPS co-pyrolysis oil with the lowest mean molecular weight of 187.85g/mol was obtained under 425ºC, 30wt% PS, and 0mL/min (Fig. 14d). It could be concluded that low temperature, high PS mass fraction, and non-sweeping atmosphere were conducive to the light WPE/WPS co-pyrolysis oil production.

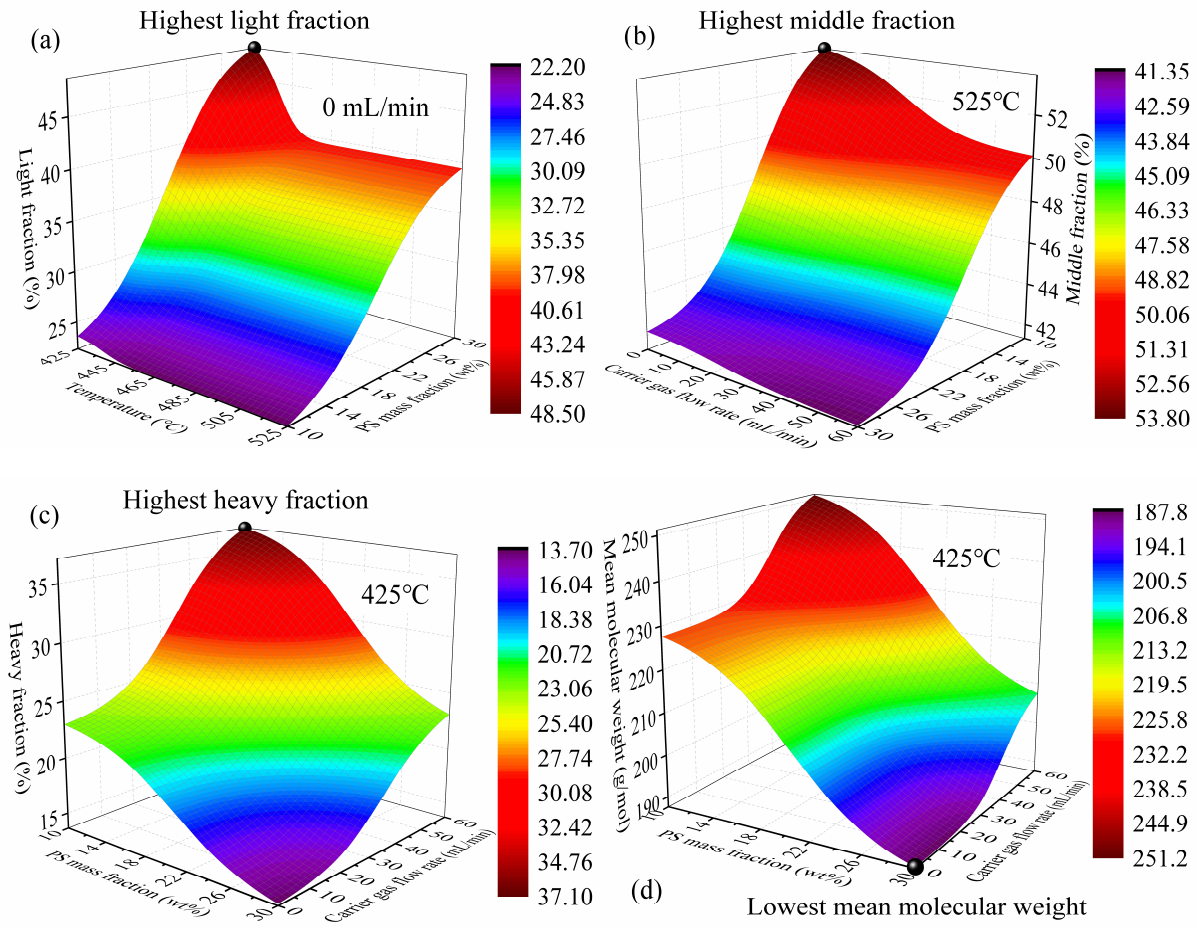

Fig. 14. ANN-GA optimized oil fractions and mean molecular weight: (a) Highest light fraction; (b) Highest middle fraction; (c) Highest heavy fraction; (d) Lowest mean molecular weight.

4. Conclusions

This study investigated the co-pyrolysis of WPE/WPS for oil production under different temperatures and carrier gas flow rates. The ratio of the real-life WPE and WPS is different in different regions. Therefore, the effect of WPE/WPS mixture composition on oil production was also studied. It was found that the WPE/WPS mixture composition and operating conditions had complex interactions on the co-pyrolysis oil yield. Therefore, a hybrid model of ANN-GA was adopted to optimize the conditions for oil production based on the central-

459 composite design. It is noteworthy that the optimized conditions in this study have limitations
460 because the experiments were performed in a bench-scale reactor. Nevertheless, the findings
461 could provide qualitative guidance for the regional industrialization of waste plastic pyrolysis.
462 ANN-GA can also be used to regulate different target products under more complicated
463 conditions due to its good robustness. This study's principal conclusions are outlined as
464 follows.

465 - The highest oil yield was 82.33wt% under 525℃, 10wt% PS, and 0mL/min. The findings
466 revealed that high temperature, low PS mass fraction, and low carrier gas flow rate were
467 conducive to a higher oil yield.
468 - The highest alkanes, alkenes, and aromatics proportions were 48.09%, 52.57%, and
469 43.73%, respectively. Additionally, the highest styrene/aromatics ratio was 55.22% under
470 the same conditions as the highest aromatics proportion (425℃, 30wt% PS, and 0mL/min).
471 - The lightest WPE/WPS co-pyrolysis oil with the lowest mean molecular weight of
472 187.85g/mol was obtained under 425℃, 30wt% PS, and 0mL/min. It could be concluded
473 that low temperature, high PS mass fraction, and low carrier gas flow rate were conducive
474 to the light WPE/WPS co-pyrolysis oil production.

475

476 **Author Information**

477 Corresponding Author *E-mail: ruming.pan@toulouse-inp.fr

478 **Competing Interest**

479 The authors declare no competing financial interest.

Acknowledgments

This work was supported by the China Scholarship Council (CSC) program (No. 201906120036).

References

[1] Plastics - the Facts 2020. PlasticsEurope (2020), https://www.plasticseurope.org/en/resources/market-data.

[2] S. Karayılan, Ö. Yılmaz, Ç. Uysal, S. Naneci. Prospective evaluation of circular economy practices within plastic packaging value chain through optimization of life cycle impacts and circularity. Resour Conserv Recycl, 173 (2021), p. 105691, https://doi.org/10.1016/j.resconrec.2021.105691.

[3] Z. Dobó, G. Kecsmár, G. Nagy, T. Koós, G. Muránszky, M. Ayari. Characterization of gasoline-like transportation fuels obtained by distillation of pyrolysis oils from plastic waste mixtures. Energ Fuel, 35 (3) (2021), pp. 2347-2356, https://doi.org/10.1021/acs.energyfuels.0c04022.

[4] M. MacLeod, H.P.H. Arp, M.B. Tekman, A. Jahnke. The global threat from plastic pollution. Science, 373 (2021), pp. 61-65, https://doi.org/10.1126/science.abg5433.

[5] S.Y. Zhao, C. Wang, B. Bai, H. Jin, W.W. Wei. Study on the polystyrene plastic degradation in supercritical water/CO2 mixed environment and carbon fixation of polystyrene plastic in CO2 environment. J Hazard Mater (2021), p. 126763, https://doi.org/10.1016/j.jhazmat.2021.126763.

[6] L.D. Ellis, N.A. Rorrer, K.P. Sullivan, M. Otto, J.E. McGeehan, Y. Román-Leshkov, N. Wierckx, G.T. Beckham. Chemical and biological catalysis for plastics recycling and upcycling. Nat Catal, 4 (2021), pp. 539-556, https://doi.org/10.1038/s41929-021-00648-4.

[7] S.M. Al-Salem, S.R. Chandrasekaran, A. Dutta, B.K. Sharma. Study of the fuel properties

505 of extracted oils obtained from low and linear low density polyethylene pyrolysis. Fuel,
506 304 (2021), p. 121396, https://doi.org/10.1016/j.fuel.2021.121396.
507 [8] L.L. Dai, N. Zhou, Y.C. Lv, K. Cobb, Y.L. Cheng, Y.P. Wang, Y.H. Liu, P. Chen, R.G. Zou,
508 H.W. Lei, R. Ruan. Pyrolysis-catalysis for waste polyolefin conversion into low aromatic
509 naphtha. Energy Convers Manag, 245 (2021), p. 114578,
510 https://doi.org/10.1016/j.enconman.2021.114578.
511 [9] S. Mazloum, Y. Aboumsallem, S. Awad, N. Allam, K. Loubar. Modelling pyrolysis
512 process for PP and HDPE inside thermogravimetric analyzer coupled with differential
513 scanning calorimeter. Int J Heat Mass Transfer, 176 (2021), p. 121468,
514 https://doi.org/10.1016/j.ijheatmasstransfer.2021.121468.
515 [10] Y.M. Wen, I.N. Zaini, S.L. Wang, W.Z. Mu, P.G. Jönsson, W.H. Yang. Synergistic effect
516 of the co-pyrolysis of cardboard and polyethylene: A kinetic and thermodynamic study.
517 Energy, 229 (2021), p. 120693, https://doi.org/10.1016/j.energy.2021.120693.
518 [11] L. Quesada, M. Calero, M.A. Martin-Lara, A. Perez, G. Blazquez. Production of an
519 alternative fuel by pyrolysis of plastic wastes mixtures. Energ Fuel, 34 (2020), pp. 1781-
520 1790, https://doi.org/10.1021/acs.energyfuels.9b03350.
521 [12] W. Luo, Z.Y. Fan, J. Wan, Q. Hu, H. Dong, X.J. Zhang, Z. Zhou. Study on the reusability
522 of kaolin as catalysts for catalytic pyrolysis of low-density polyethylene. Fuel, 302 (2021),
523 p. 121164, https://doi.org/10.1016/j.fuel.2021.121164.
524 [13] K.B. Park, Y.S. Jeong, B. Guzelciftci, J.S. Kim. Characteristics of a new type continuous
525 two-stage pyrolysis of waste polyethylene. Energy, 166 (2019), pp. 343-351,

https://doi.org/10.1016/j.energy.2018.10.078.

[14] S.M. Al-Salem, A. Dutta. Wax recovery from the pyrolysis of virgin and waste plastics. Ind Eng Chem Res, 60 (22) (2021), pp. 8301-8309, https://doi.org/10.1021/acs.iecr.1c01176.

[15] J. Nisar, G. Ali, A. Shah, M. Iqbal, R.A. Khan, Sirajuddin, F. Anwar, R. Ullah, M.S. Akhter. Fuel production from waste polystyrene via pyrolysis: Kinetics and products distribution. Waste Manage, 88 (2019), pp. 236-247, https://doi.org/10.1016/j.wasman.2019.03.035.

[16] M.N. Siddiqui, H.H. Redhwi. Pyrolysis of mixed plastics for the recovery of useful products. Fuel Process Technol, 90 (4) (2009), pp. 545-552, https://doi.org/10.1016/j.fuproc.2009.01.003.

[17] P.T. Williams, E.A. Williams. Interaction of plastics in mixed-plastics pyrolysis. Energ Fuel, 13 (1) (1999), pp. 188-196, https://doi.org/10.1021/ef980163x.

[18] Klaimy, S., Lamonier, J.F., Casetta, M., Heymans, S. and Duquesne, S., 2021. Recycling of plastic waste using flash pyrolysis–Effect of mixture composition. Polymer Degradation and Stability, 187, p.109540. https://doi.org/10.1016/j.polymdegradstab.2021.109540

[19] Saad, J.M., Williams, P.T., Zhang, Y.S., Yao, D., Yang, H. and Zhou, H., 2021. Comparison of waste plastics pyrolysis under nitrogen and carbon dioxide atmospheres: A thermogravimetric and kinetic study. Journal of Analytical and Applied Pyrolysis, 156, p.105135. https://doi.org/10.1016/j.jaap.2021.105135

547 [20] Kusenberg, M., Zayoud, A., Roosen, M., Thi, H.D., Abbas-Abadi, M.S., Eschenbacher, A.,
548 Kresovic, U., De Meester, S. and Van Geem, K.M., 2022. A comprehensive experimental
549 investigation of plastic waste pyrolysis oil quality and its dependence on the plastic waste
550 composition. Fuel Processing Technology, 227, p.107090.
551 https://doi.org/10.1016/j.fuproc.2021.107090
552 [21] Dyer, A.C., Nahil, M.A. and Williams, P.T., 2021. Catalytic co-pyrolysis of biomass and
553 waste plastics as a route to upgraded bio-oil. Journal of the Energy Institute, 97, pp.27-36.
554 https://doi.org/10.1016/j.joei.2021.03.022
555 [22] R.M. Pan, M.F. Martins, G. Debenest. Pyrolysis of waste polyethylene in a semi-batch
556 reactor to produce liquid fuel: Optimization of operating conditions. Energy Convers
557 Manag, 237 (2021), p. 114114, https://doi.org/10.1016/j.enconman.2021.114114.
558 [23] I. Muhammad, N. Makwashi, G. Manos. Catalytic degradation of linear low-density
559 polyethylene over HY-zeolite via pre-degradation method. J Anal Appl Pyrolysis, 138
560 (2019), pp. 10-21, https://doi.org/10.1016/j.jaap.2018.11.025.
561 [24] Janarthanan, R., Maheshwari, R.U., Shukla, P.K., Shukla, P.K., Mirjalili, S. and Kumar,
562 M., 2021. Intelligent Detection of the PV Faults Based on Artificial Neural Network and
563 Type 2 Fuzzy Systems. Energies, 14(20), p.6584. https://doi.org/10.3390/en14206584
564 [25] Neshat, M., Nezhad, M.M., Abbasnejad, E., Mirjalili, S., Groppi, D., Heydari, A.,
565 Tjernberg, L.B., Garcia, D.A., Alexander, B., Shi, Q. and Wagner, M., 2021. Wind turbine
566 power output prediction using a new hybrid neuro-evolutionary method. Energy, 229,
567 p.120617. https://doi.org/10.1016/j.energy.2021.120617

568 [26] Neshat, M., Nezhad, M.M., Abbasnejad, E., Mirjalili, S., Tjernberg, L.B., Garcia, D.A.,
569 Alexander, B. and Wagner, M., 2021. A deep learning-based evolutionary model for
570 short-term wind speed forecasting: A case study of the Lillgrund offshore wind farm.
571 Energy Conversion and Management, 236, p.114002.
572 https://doi.org/10.1016/j.enconman.2021.114002
573 [27] Khatir, S., Tiachacht, S., Le Thanh, C., Ghandourah, E., Mirjalili, S. and Wahab, M.A.,
574 2021. An improved Artificial Neural Network using Arithmetic Optimization Algorithm
575 for damage assessment in FGM composite plates. Composite Structures, 273, p.114287.
576 https://doi.org/10.1016/j.compstruct.2021.114287
577 [28] Kundu, R., Singh, P.K., Mirjalili, S. and Sarkar, R., 2021. COVID-19 detection from lung
578 CT-Scans using a fuzzy integral-based CNN ensemble. Computers in Biology and
579 Medicine, 138, p.104895. https://doi.org/10.1016/j.compbiomed.2021.104895
580 [29] Ala, A., Alsaadi, F.E., Ahmadi, M. and Mirjalili, S., 2021. Optimization of an
581 appointment scheduling problem for healthcare systems based on the quality of fairness
582 service using whale optimization algorithm and NSGA-II. Scientific Reports, 11(1), pp.1-
583 19. https://doi.org/10.1038/s41598-021-98851-7
584 [30] Pan, R., Duque, J.V.F. and Debenest, G., 2022. Waste Plastic Thermal Pyrolysis Analysis
585 by a Neural Fuzzy Model Coupled with a Genetic Algorithm. Waste and Biomass
586 Valorization, 13(1), pp.135-148. https://doi.org/10.1007/s12649-021-01522-x
587 [31] L. Quesada, A. Perez, V. Godoy, F.J. Peula, M. Calero, G. Blazquez. Optimization of the
588 pyrolysis process of a plastic waste to obtain a liquid fuel using different mathematical

models. Energy Convers Manag, 188 (2019), pp. 19-26, https://doi.org/10.1016/j.enconman.2019.03.054.

[32] C.X. Wang, H.W. Lei, M.R.O. Qian, E.G. Huo, Y.F. Zhao, Q.F. Zhang, et al. Application of highly stable biochar catalysts for efficient pyrolysis of plastics: A readily accessible potential solution to a global waste crisis. Sustain Energy Fuels, 4 (2020), pp. 4614-4624, https://doi.org/10.1039/D0SE00652A.

[33] S. Uslu. Optimization of diesel engine operating parameters fueled with palm oil-diesel blend: Comparative evaluation between response surface methodology (RSM) and artificial neural network (ANN). Fuel, 276 (2020), p. 117990, https://doi.org/10.1016/j.fuel.2020.117990.

[34] J.A. Onwudili, N. Insura, P.T. Williams. Composition of products from the pyrolysis of polyethylene and polystyrene in a closed batch reactor: Effects of temperature and residence time. J Anal Appl Pyrolysis, 86 (2009), pp. 293-303, https://doi.org/10.1016/j.jaap.2009.07.008.

[35] P.T. Williams, E. Slaney. Analysis of products from the pyrolysis and liquefaction of single plastics and waste plastic mixtures. Resour Conserv Recycl, 51 (4) (2007), pp. 754-769, https://doi.org/10.1016/j.resconrec.2006.12.002.

[36] Q.H. Tang, Y.Q. Chen, H.P. Yang, M. Liu, H.Y. Xiao, S.R. Wang, H.P. Chen, S.R. Naqvi. Machine learning prediction of pyrolytic gas yield and compositions with feature reduction methods: Effects of pyrolysis conditions and biomass characteristics. Bioresour Technol, 339 (2021), p. 125581, https://doi.org/10.1016/j.biortech.2021.125581.

610 [37] D. Kwon, S. Jung, K.Y.A. Lin, Y.F. Tsang, Y.K. Park, E.E. Kwon. Synergistic effects of
611 CO2 on complete thermal degradation of plastic waste mixture through a catalytic
612 pyrolysis platform: A case study of disposable diaper. J Hazard Mater, 419 (2021), p.
613 126537, https://doi.org/10.1016/j.jhazmat.2021.126537.
614 [38] D.K. Hong, P. Li, T. Si, X. Guo. ReaxFF simulations of the synergistic effect mechanisms
615 during co-pyrolysis of coal and polyethylene/polystyrene. Energy, 218 (2021), p. 119553,
616 https://doi.org/10.1016/j.energy.2020.119553.
617 [39] Y.M. Wen, S.L. Wang, W.Z. Mu, W.H. Yang, P.G. Jönsson. Pyrolysis performance of peat
618 moss: A simultaneous in-situ thermal analysis and bench-scale experimental study. Fuel,
619 277 (2020), p. 118173, https://doi.org/10.1016/j.fuel.2020.118173.
620 [40] Z.Z. Chen, X.R. Zhang, L. Che, H.H. Peng, S.X. Zhu, F. Yang, X. Zhang. Effect of
621 volatile reactions on oil production and composition in thermal and catalytic pyrolysis of
622 polyethylene. Fuel, 271 (2020), p. 117308, https://doi.org/10.1016/j.fuel.2020.117308.
623 [41] J. Wang, J.C. Jiang, J.H. Ding, X.B. Wang, Y.J. Sun, R. Ruan, A.J. Ragauskas, Y.S. Ok,
624 D.C.W. Tsang. Promoting Diels-Alder reactions to produce bio-BTX: Co-aromatization
625 of textile waste and plastic waste over USY zeolite. J Clean Prod, 314 (2021), p. 127966,
626 https://doi.org/10.1016/j.jclepro.2021.127966.
627 [42] F.F. Xu, X. Ming, R. Jia, M. Zhao, B. Wang, Y.Y. Qiao, Y.Y. Tian. Effects of operating
628 parameters on products yield and volatiles composition during fast pyrolysis of food
629 waste in the presence of hydrogen. Fuel Process Technol, 210 (2020), p. 106558,
630 https://doi.org/10.1016/j.fuproc.2020.106558.

631 [43] H.S. Choi, Y.S. Choi, H.C. Park. Fast pyrolysis characteristics of lignocellulosic biomass
632 with varying reaction conditions. Renew Energy, 42 (2012), pp. 131-135,
633 https://doi.org/10.1016/j.renene.2011.08.049.
634 [44] R.K. Singh, B. Ruj, A.K. Sadhukhan, P. Gupta. Thermal degradation of waste plastics
635 under non-sweeping atmosphere: Part 1: Effect of temperature, product optimization, and
636 degradation mechanism. J Environ Manage, 239 (2019), pp. 395-406,
637 https://doi.org/10.1016/j.jenvman.2019.03.067.
638 [45] S.D.A. Sharuddin, F. Abnisa, W.M.A.W. Daud, M.K. Aroua. A review on pyrolysis of
639 plastic wastes. Energy Convers Manag, 115 (2016), pp. 308-326,
640 https://doi.org/10.1016/j.enconman.2016.02.037.
641 [46] J. Baena-Gonzalez, A. Santamaria-Echart, J.L. Aguirre, S. Gonzalez. Chemical recycling
642 of plastic waste: Bitumen, solvents, and polystyrene from pyrolysis oil. Waste Manage,
643 118 (2020), pp. 139-149, https://doi.org/10.1016/j.wasman.2020.08.035.
644 [47] C.H. Gu, X.H. Wang, Q.S. Song, H.W. Li, Y. Qiao. Prediction of gas-liquid-solid product
645 distribution after solid waste pyrolysis process based on artificial neural network model.
646 Int J Energy Res, 45 (9) (2021), pp. 13786-13800, https://doi.org/10.1002/er.6707.
647 [48] K.H. Lee, D.H. Shin. Characteristics of liquid product from the pyrolysis of waste plastic
648 mixture at low and high temperatures: Influence of lapse time of reaction. Waste Manage,
649 27 (2) (2007), pp. 168-176, https://doi.org/10.1016/j.wasman.2005.12.017.
650 [49] F. Pinto, F. Paradela, I. Gulyurtlu, A.M. Ramos. Prediction of liquid yields from the
651 pyrolysis of waste mixtures using response surface methodology. Fuel Process Technol,

652 116 (2013), pp. 271-283, https://doi.org/10.1016/j.fuproc.2013.07.012.
653 [50] A. Heidari, R. Stahl, H. Younesi, A. Rashidi, N. Troeger, A.A. Ghoreyshi. Effect of
654 process conditions on product yield and composition of fast pyrolysis of Eucalyptus
655 grandis in fluidized bed reactor. J Ind Eng Chem, 20 (4) (2014), pp. 2594-2602,
656 https://doi.org/10.1016/j.jiec.2013.10.046.
657 [51] M.S. Abbas-Abadi, K.M. Van Geem, M. Fathi, H. Bazgir, M. Ghadiri. The pyrolysis of
658 oak with polyethylene, polypropylene and polystyrene using fixed bed and stirred
659 reactors and TGA instrument. Energy, 232 (2021), p. 121085,
660 https://doi.org/10.1016/j.energy.2021.121085.
661 [52] A.K. Varma, P. Mondal. Pyrolysis of sugarcane bagasse in semi batch reactor: Effects of
662 process parameters on product yields and characterization of products. Ind Crops Prod,
663 95 (2017), pp. 704-717, https://doi.org/10.1016/j.indcrop.2016.11.039.
664 [53] A. Trubetskaya, P.A. Jensen, A.D. Jensen, M. Steibel, H. Spliethoff, P. Glarborg.
665 Influence of fast pyrolysis conditions on yield and structural transformation of biomass
666 chars. Fuel Process Technol, 140 (2015), pp. 205-214,
667 https://doi.org/10.1016/j.fuproc.2015.08.034.
668 [54] K.B. Ansari, S.Z. Hassan, Bhoi, R., E. Ahmad. Co-pyrolysis of biomass and plastic
669 wastes: A review on reactants synergy, catalyst impact, process parameter, hydrocarbon
670 fuel potential, COVID-19. J Environ Chem Eng, 9 (6) (2021), p. 106436.
671 https://doi.org/10.1016/j.jece.2021.106436.
672 [55] F. Abnisa, P.A. Alaba. Recovery of liquid fuel from fossil-based solid wastes via pyrolysis

technique: A review. J Environ Chem Eng, 9 (6) (2021), p. 106593. https://doi.org/10.1016/j.jece.2021.106593.

[56] J. Haydary, D. Susa, V. Gelinger, F. Čacho, Pyrolysis of automobile shredder residue in a laboratory scale screw type reactor. J Environ Chem Eng, 4 (1) (2016), pp. 965-972. https://doi.org/10.1016/j.jece.2015.12.038.

[57] J. Su, C. Fang, M. Yang, C. You, Q. Lin, X. Zhou, H. Li. Catalytic pyrolysis of waste packaging polyethylene using AlCl3-NaCl eutectic salt as catalyst. J Anal Appl Pyrolysis, 139 (2019), pp. 274-281, https://doi.org/10.1016/j.jaap.2019.02.015.

[58] P. Das, P. Tiwari. The effect of slow pyrolysis on the conversion of packaging waste plastics (PE and PP) into fuel. Waste Manage, 79 (2018), pp. 615-624, https://doi.org/10.1016/j.wasman.2018.08.021.

[59] M. Maniscalco, F. La Paglia, P. Iannotta, G. Caputo, F. Scargiali, F. Grisafi, A. Brucato. Slow pyrolysis of an LDPE/PP mixture: Kinetics and process performance. J Energy Inst, 96 (2021), pp. 234-241. https://doi.org/10.1016/j.joei.2021.03.006.

Waste plastics recovered from MSW

Pyrolysis

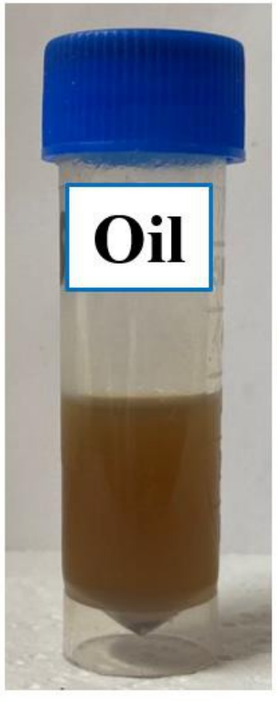

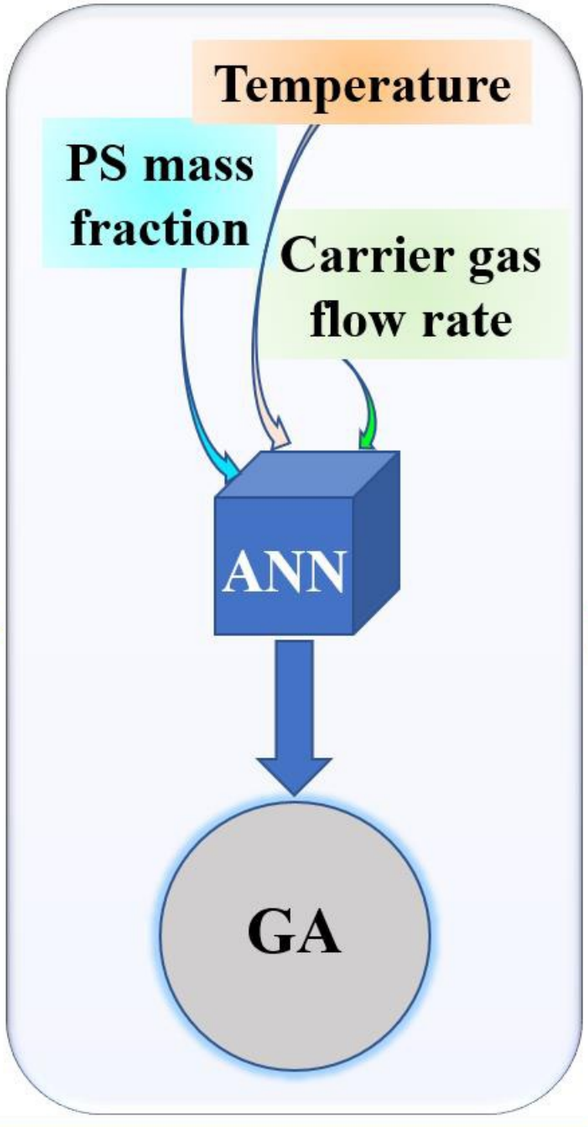

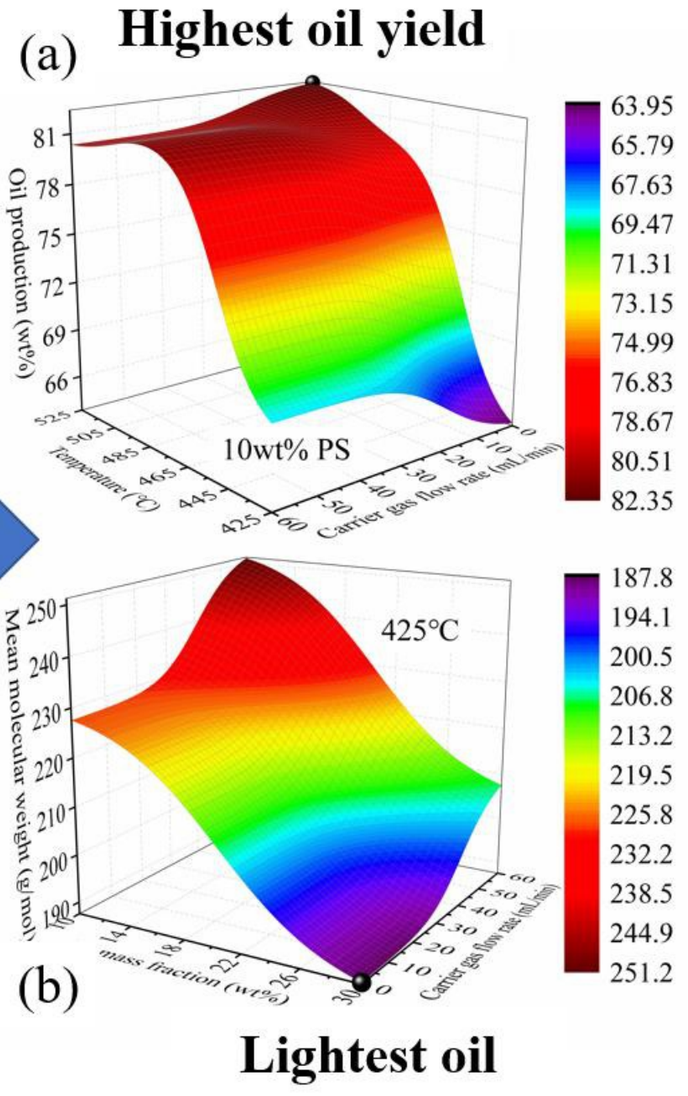

WPE/WPS co-pyrolysis for oil production